Bose-Einstein condensates in spin-orbit-coupled optical lattices: Flat bands and superfluidity

Yongping Zhang[1] and Chuanwei Zhang[1,2,*]

[1]*Department of Physics and Astronomy, Washington State University, Pullman, Washington 99164, USA*

[2]*Department of Physics, The University of Texas at Dallas, Richardson, Texas 75080, USA*

(Received 2 January 2013; published 13 February 2013)

Recently spin-orbit (SO)-coupled superfluids in free space or harmonic traps have been extensively studied, motivated by the recent experimental realization of SO coupling for Bose-Einstein condensates (BEC). However, the rich physics of SO-coupled BEC in optical lattices has been largely unexplored. In this paper, we show that in a suitable parameter region the lowest Bloch state forms an isolated flat band in a one-dimensional SO-coupled optical lattice, which thus provides an experimentally feasible platform for exploring the recently celebrated topological flatband physics in lattice systems. We show that the flat band is preserved even with the mean-field interaction in BEC. We investigate the superfluidity of the BEC in SO-coupled lattices through dynamical and Landau stability analysis, and show that the BEC is stable on the whole flat band.

DOI: 10.1103/PhysRevA.87.023611 PACS number(s): 67.85.−d, 03.75.Lm, 03.75.Mn, 71.70.Ej

I. INTRODUCTION

Flat bands possess macroscopic level degeneracy because of their flat energy dispersion. They play a crucial role in important physical phenomena such as fractional quantum Hall effects where a large magnetic field applied on a two-dimensional electron gas induces flat Landau levels [1]. The flat band physics is also greatly enriched recently by studying various lattice models where flat bands can be generated through geometrical frustration of hopping [2,3] (e.g., kagomé lattice), the destructive interference between nearest-neighbor and higher-order tunnelings (such as next-nearest neighbor) [4–6], or the p-orbital physics [7]. In particular, isolated flat bands in lattices with nontrivial topological properties have attracted much attention in condensed matter physics for their applications in engineering fractional topological quantum insulators [8–14] without Landau levels.

However, most previous lattice models for generating flat bands involve either high-orbital bands or high-order tunnelings, which are generally very challenging in experiments. In this paper, we propose an experimentally feasible route for generating isolated flat bands using cold atoms in spin-orbit (SO)-coupled weak optical lattices. Our work is motivated by the recent experimental realization of SO coupling for BEC [15], which opens a completely new avenue for exploring SO-coupled superfluids [16]. In particular, SO-coupled BEC and degenerated Fermi gases in free space and harmonic traps have been extensively investigated recently [17–39]. However, ultracold atoms in SO-coupled optical lattices have been largely unexplored [40]. We show that the combination of SO coupling, Zeeman field, and optical lattice potential can yield isolated flat bands where topological properties may originate from the SO coupling [41,42]. In regular optical lattices, the minimum of the lowest Bloch band locates at the center of the first Brillouin zone (BZ), while the maximum locates at the edge [43]. In SO-coupled optical lattices, the minimum may locate at the edge and the peak at the center. The height of the central peak can be reduced with increasing Zeeman field, leading to decreasing bandwidth and flat bands in a certain parameter region. We note that such flat band dispersion has been observed very recently in experiments in SO-coupled optical lattices using ^{6}Li Fermi atoms [44].

We first investigate a single atom in a one-dimensional (1D) SO-coupled weak optical lattice to illustrate the mechanism for generating isolated flat bands. The atom-atom interaction in BEC is then taken into account using the mean-field Gross-Pitaevskii (GP) equation [45]. The nonlinear interaction reduces the band flatness, but does not fully destroy the isolated flat bands. The combination of nonlinear interaction and flat bands may lead to rich and interesting physics. In particular, the instability of the nonlinear Bloch waves is very important because it directly relates to the breakdown of superfluidity of the BEC [46–56]. In SO-coupled optical lattices, the nonzero momentum of the energy minimum of the lowest Bloch band and the existence of flat bands make their stability very different from regular optical lattices. For instance, the nonlinear Bloch waves can be stable in the whole BZ in the flat band region.

The rest of the paper is organized as follows. In Sec. II, we present the flat band structure in SO-coupled optical lattices. In Sec. III, we discuss the effects of mean-field interactions and analyze the stability of the BEC in SO-coupled optical lattices. Sec. IV is the conclusion.

II. FLAT BANDS IN SO-COUPLED OPTICAL LATTICES

We consider a BEC confined in a 1D optical lattice potential $V_0 \sin^2(k_L x)$ along the x direction with V_0 as the lattice depth. In experiments, the lattice potential can be created by a standing wave formed by two lasers propagating along different directions [52] (see Fig. 1). The effective wave vector of the lattice is $k_L = 2\pi \sin(\theta_L/2)/\lambda_L$, where λ_L is the wavelength of the lasers and θ_L is the angle between two lasers. The SO coupling for BEC has been realized in experiments using two counterpropagating Raman lasers [15], yielding the single-particle Hamiltonian

$$H_0 = \frac{p^2}{2m} + \gamma p\sigma_z + \Omega\sigma_x, \tag{1}$$

*Corresponding author: chuanwei.zhang@utdallas.edu

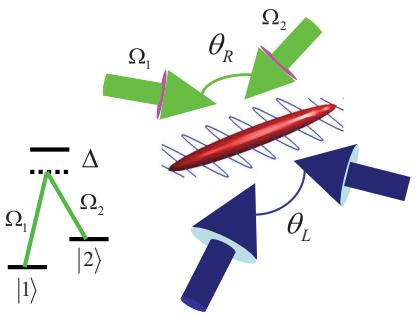

FIG. 1. (Color online) Laser setup for implementing 1D SO-coupled optical lattices. Ω_1 and Ω_2 are the Rabi frequencies of the Raman lasers for generating SO coupling. The other two laser beams generate the optical lattice.

where p is the atom momentum along the x direction, and σ is the Pauli matrix. The SO-coupling strength $\gamma = \hbar k_R/m$ with $k_R = 2\pi \sin(\theta_R/2)/\lambda_R$, λ_R is the wavelength of the Raman lasers, and θ_R is the angle between Raman beams. Ω is the Rabi frequency and acts as a Zeeman field. The units of the energy and length are chosen as the recoil energy $2E_L = \hbar^2 k_L^2/m$ and $1/k_L$, respectively, for the numerical calculation. Under these units, the single-particle Hamiltonian is dimensionless with $\gamma = k_R/k_L = \sin(\theta_R/2)\lambda_L/\sin(\theta_L/2)\lambda_R$ and the optical lattice potential $V_0 \sin^2(x)$.

Without optical lattice potentials, the single-particle Hamiltonian H_0 has two SO energy bands $\mu_\pm(k)$ [shown in Fig. 2(a)] due to the lift of the spin degeneracy by the SO and Zeeman field. A gap 2Ω between these two bands is opened at $k = 0$ by the Zeeman field Ω. In the lower band, there are two energy minima at $k_{\min} = \pm\sqrt{\gamma^2 - \Omega^2/\gamma^2}$ and one peak at $k = 0$. With increasing Ω, the distance between two $k_{\min}$ shrinks, and the height of the central peak decreases. At a critical value $\Omega_c = \gamma^2$ and beyond, two $k_{\min}$ merge to one point at $k_{\min} = 0$, and the central peak vanishes.

In the presence of periodic lattice potentials [i.e., consider the Hamiltonian $H_0 + V_0 \sin^2(x)$], the eigenenergies of the single-particle Hamiltonian form the Bloch energy bands [43]. To generate an isolated flat band, it is necessary to reduce the energy at both the edge and the center of the first BZ with respect to the band minimum, which can be realized through a combination of SO coupling, Zeeman field, and lattice potential. Specifically, the periodic lattice potential can

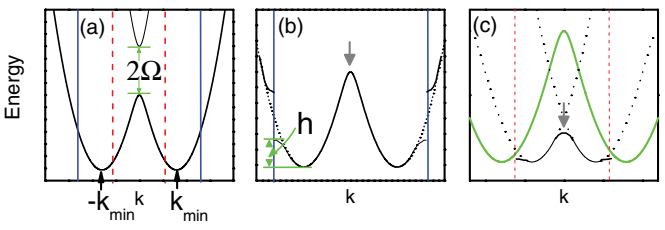

FIG. 2. (Color online) Illustration of the formation of isolated flat bands. (a) Energy dispersion $\mu_\pm(k)$ of the single-particle Hamiltonian H_0. The vertical solid (or dashed) lines correspond to the edges of the first BZ. (b) Lowest band for $\gamma < 1$. The gray arrow indicates the suppression of the central peak with increasing Ω. (c) The formation of the lowest band for $\gamma \geqslant 1$. The solid (green) line is $\mu_-(k)$, while the dotted lines are $\mu_-(k \pm 2)$.

open an energy gap at the edge of the first BZ, which lowers the energy difference between the edge and the band minimum (denoted as h). When the original band minimum is close to the edge, the band edge becomes the band minimum (i.e., $h = 0$). On the other hand, the height of the central peak decreases with increasing Ω. The bandwidth should be determined by the larger value of h and the central peak height.

The flat band generation mechanism is slightly different in two different regions: $\gamma < 1$ and $\gamma \geqslant 1$. For $\gamma < 1$, $k_{\min} = \gamma$ at $\Omega = 0$ is within the first BZ [Fig. 2(b)]. If γ is close to 1, h should be zero and the bandwidth is determined by the central peak height, which can be greatly reduced with increasing Ω. Therefore the lowest band could be very flat for a certain parameter region. However, if γ is much smaller than 1, h becomes a large value, and the width of the lowest band cannot be squeezed to the flat region. For $\gamma \geqslant 1$, $k_{\min}$ of H_0 lays outside of the first BZ. In this case, the lowest band is formed through folding the energy spectrum into the first BZ [i.e., shift the energy band of H_0 by a lattice vector; see Fig. 2(c)]. The band minima now locate at $k_{\min} \mp 2$, and the physics is similar to that in $\gamma < 1$. However, there is one major difference between $\gamma \geqslant 1$ and $\gamma < 1$. For $\gamma \geqslant 1$, the minimum of the lowest band first shift towards the edge of the first BZ when Ω increases from 0. Therefore at a certain range of Ω, the band minimum always stays at the band edge and the flat band can be realized by suppressing the central peak with increasing Ω. We emphasize that the resulting flat band is the ground state of the SO-coupled lattice, which further enhances its experimental feasibility because atoms are usually adiabatically loaded to the lowest band in experiments [52]. Such SO mechanism for flat bands is very different from previous schemes in literature using high-order tunneling or high-orbital physics.

The above intuitive physical picture agrees well with the numerical results. Using the Bloch theorem, the Bloch waves can be written as $\Psi(x,t) = \Phi(x)\exp[-i\mu(k)t + ikx]$, where $\Phi(x)$ is the periodic part of the Bloch wave function, and $\mu(k)$ is the eigenenergy, which can be calculated using the standard central equation. We measure the flatness of the lowest Bloch band by the ratio R of the gap between the lowest and first excited bands to the width of the lowest band. In Fig. 3, we plot the flatness R with respect to Ω for two different γ. In the calculation, we use $\lambda_R = 804.1$ nm and $\lambda_L = 840$ nm which are typical for ^{87}Rb atoms in experiments [15]. The optical lattice potential is weak, $V_0 = 2E_L$, to make sure the flat band does not come from the high lattice potential. For simplicity we choose $\theta_L = \pi$, and consider two different θ_R: $\theta_R = \pi$ corresponds to $\gamma = 0.74$ [in Fig. 3(a)], and $\theta_R = \pi/2$ corresponds to $\gamma = 1.05$ [in Fig. 3(b)]. We see the maximum flatness can reach nearly 20/1 for $\gamma = 0.74$ and 170/1 for $\gamma = 1.05$. The suppression of the flatness for $\gamma = 0.74 < 1$ agrees with our intuitive physical picture: The band minimum for $\gamma = 0.74$ is a little bit far from the edge of the first BZ, therefore the lowest band cannot be squeezed to exactly flat. In experiments, γ can be varied using laser setups with different θ_L and θ_R or through a fast modulation of the laser intensities of the Raman lasers [32]. The dependence of the maximum flatness on the SO coupling γ is plotted in Fig. 3(c). With increasing SO coupling, the lowest band becomes more flat.

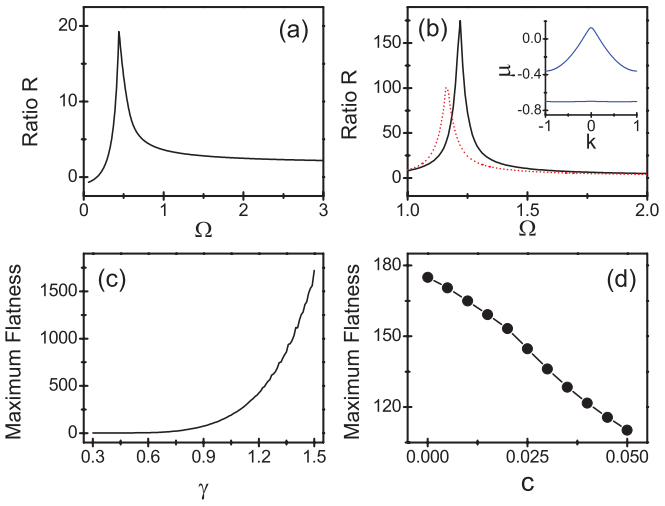

FIG. 3. (Color online) Flatness (ratio R) of the lowest Bloch band. $V_0 = 1$. (a) $\gamma = 0.74$ and $c = 0$. (b) $\gamma = 1.05$. Solid line: $c = 0$; dashed line: $c = 0.05$. The inset is a typical example of flat band in the nonlinear Bloch spectrum with $\Omega = 1.15$, $c = 0.05$. (c) Plot of the dependence of the maximum flatness on γ with $c = 0$. (d) The dependence of the maximum flatness on c with $\gamma = 1.05$.

III. STABILITY OF BEC IN SO-COUPLED OPTICAL LATTICES

So far the study has been limited to the linear case, i.e., a single atom, while the interactions between atoms in BEC may play a major role on the dynamics of BEC. In the presence of a weak lattice potential, the mean-field theory still applies and the dynamics of BEC in SO-coupled optical lattices can be described by the nonlinear GP equation

$$i\frac{\partial \Psi}{\partial t} = H_0\Psi + V_0\sin^2(x)\Psi + c(|\Psi_1|^2 + |\Psi_2|^2)\Psi, \qquad (2)$$

where $\Psi = (\Psi_1, \Psi_2)^T$ is the two-component wave function of the BEC. The unit of time is $m/\hbar k_L^2$ and the wave function is normalized through $\int dx(|\Psi_1|^2 + |\Psi_2|^2) = 1$ in one unit cell. The dimensionless interaction coefficient $c = \hbar\sqrt{\omega_y\omega_z}k_L aN/E_L$, where N is the atom number in one unit cell, a is the s-wave scattering length, and ω_y and ω_z are the trapping frequencies in the transverse directions. We consider a 1D BEC confined in an elongated cigar-shaped trap with high transverse trapping frequencies (y and z directions), while the trapping potential in the longitudinal direction (x) is negligible. We also assume the interaction coefficients between atoms are the same for different hyperfine states, which is a very good approximation because their difference is very small [57].

Even in the presence of nonlinear terms, the solution of the GPE is still the Bloch wave in a periodic optical lattice [46,47]. The repulsive interaction shifts the Bloch spectrum upwards, and modifies each band dispersion and energy gap at the same time. However, isolated flat bands still exist in the presence of nonlinearity, as shown in Fig. 3(b) where the flatness of the lowest band is plotted for $c = 0.05$. Compared with the linear case $c = 0$, the flatness of the nonlinear flat band decreases with increasing nonlinearity [Fig. 3(d)] and the maximum flatness is shifted towards a smaller value of Ω. A typical example of the nonlinear Bloch spectrum with an isolated flat band is shown in the inset of Fig. 3(b).

The combination of nonlinear interaction and flat bands may lead to various important phenomena, one of which is the superfluidity of the BEC in SO-coupled optical lattices. For BEC in optical lattices, the breakdown of superfluidity may be caused by two different types of instabilities of the BEC, dynamical instability and Landau instability, both of which have been extensively studied in theory and experiments [46–56]. The existence of SO coupling and flat bands may significantly modify the superfluidity of the BEC. The stability analysis can be performed through Bogoliubov theory, where quasiparticle excitations induced by perturbations are taken into account through a small modification of the wave function $\Psi_i(x,t) = [\Phi_i(x) + \Delta\Phi_i(x,t)]\exp(-i\mu t + ikx)$, where $\Phi_i(x)$ is the ground state of the BEC, $\Delta\Phi_i(x,t) = u_i(x)\exp(iqx - i\delta t) + w_i^*(x)\exp(-iqx + i\delta^* t)$, q and δ are the wave vector and energy of the quasiparticle excitations, while u_i and w_i are the quasiparticle amplitudes. Substituting the modified wave function into the Gross-Pitaevskii equation (GPE), and linearizing the GPE with respect to u_i and w_i, we obtain Bogoliubov–de Gennes (BdG) equations $\delta\varphi = \mathcal{M}\varphi$ with $\varphi = (u_1, w_1, u_2, w_2)^T$, where the matrix

$$\mathcal{M} = \begin{pmatrix} \mathcal{A}_{12} & \mathcal{B}_{12} \\ \mathcal{B}_{21} & \mathcal{A}_{21} \end{pmatrix}, \qquad (3)$$

with

$$\mathcal{A}_{mn} = \begin{pmatrix} \mathcal{L}^{(mn)}(q+k) & c\Phi_m \\ -c\Phi_m^* & \mathcal{L}^{(mn)}(q-k) \end{pmatrix},$$

$$\mathcal{B}_{mn} = \begin{pmatrix} \Omega + c\Phi_m\Phi_n^* & c\Phi_m\Phi_n \\ -c\Phi_m^*\Phi_n^* & -\Omega - c\Phi_m^*\Phi_n \end{pmatrix}.$$

Here $\mathcal{L}^{(mn)}(k) = -1/2(\partial/\partial x + ik)^2 + V_0\sin^2(x) - i\gamma(\partial/\partial x + ik) - \mu + 2c|\Phi_m|^2 + c|\Phi_n|^2$. Because the matrix $\mathcal{M}$ is not Hermitian, its eigenvalues may be imaginary. The dynamical instability is defined if $\mathcal{M}$ has one or more nonzero imaginary eigenvalues. In this case, the instability is characterized by the exponential growth of the perturbation. The nonlinear Bloch wave is dynamically stable if all eigenvalues are real numbers. On the other hand, the Landau instability can be studied by solving the BdG equation [46], $\beta\varphi = \tau_z\mathcal{M}\varphi$ with $\tau_z = \mathbf{I}\otimes\sigma_z$. The nonlinear Bloch wave Φ_i is said to be Landau instable if one or more eigenvalues of $\tau_z\mathcal{M}$ are negative. Physically, the nonlinear Bloch wave with Landau instability is not the local energy minimum of the system.

We systematically study the stability of nonlinear Bloch waves at the lowest Bloch band for various parameters. A typical example of the dynamical and Landau instability of the lowest band is shown in Figs. 4(a) and 4(b). Due to the symmetry in the plane (q,k), we only show the region $0 \leqslant q \leqslant 1$ and $0 \leqslant k \leqslant 1$. In Fig. 4(a), the maximum of the imaginary part of δ is shown. The BEC in the region with nonzero values is dynamically unstable. There is a critical k_{c1} beyond which Bloch waves become dynamically stable. In Fig. 4(b), the negative maximum of β is plotted, and nonzero values indicate the Landau instability. There is also a critical k_{c2} beyond which Bloch waves are the local energy minimum.

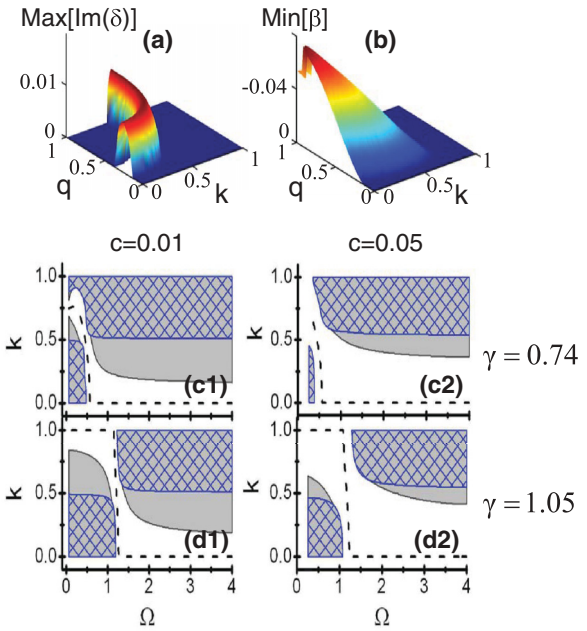

FIG. 4. (Color online) Instability of the lowest Bloch band. (a), (b) Plots of the maximum of Im(δ) for dynamical instability (a) and the negative maximum of β for Landau instability (b). $V_0 = 1$, $c = 0.01$, $\gamma = 1.05$, and $\Omega = 0.8$. (c1), (c2), (d1), (d2) Instability regions in the (k,Ω) plane. Dashed lines: the minimum of the lowest band; blue grids: dynamical instability regions; gray shadows: Landau instability regions.

In Figs. 4(c) and 4(d), we plot the dynamical and Landau instability region for different nonlinearity, SO coupling, and Zeeman field. For BEC in a regular optical lattice, the energy minimum of the lowest band locates at $k = 0$, and the Bloch waves in the region around $k = 0$ are stable, while in SO-coupled optical lattices, the energy minimum of the lowest band may not locate at $k = 0$, therefore we expect the stability domains should change accordingly, as clearly shown in Figs. 4(c) and 4(d). For $\gamma = 0.74 < 1$ in Figs. 4(c1) and 4(c2), the minimum of the lowest band (dashed lines) shrinks to $k = 0$ with increasing Ω, and the abrupt change of the energy minimum corresponds to the flat band region. When γ is close to one-half of the first BZ, e.g., $\gamma = 1.05$ in Figs. 4(d1) and 4(d2), the energy minimum initially stays at the edge of the first BZ $k = 1$. In the flat band region, the energy minimum quickly moves to $k = 0$. For a larger γ, the energy minimum initially increases from a value smaller than $k = 1$ to the edge with increasing Ω, stays there for a certain range of Ω, and then suddenly moves to $k = 0$. The numerical results agree with the natural expectation that Bloch waves surrounding the minimum of the lowest band are stable, as shown in Figs. 4(c) and 4(d). However, we see the whole band is stable in the flat band region, which means that the superfluidity of BEC with any momentum in the flat band is conserved. There are two other properties: (1) the region of dynamic instability is always smaller than the region of Landau instability and (2) the stable region increases for a larger nonlinear coefficient c. These two properties are the same as those for BEC in regular lattices [46,47].

IV. CONCLUSION

In summary, we show that the combination of SO coupling, Zeeman field, and optical lattice can generate flat ground state energy bands where the superfluid of the BEC is stable in the whole band region. Our proposed SO-coupling mechanism, when generalized to 2D, may provide an experimentally feasible route for generating chiral flat bands and studying relevant fractional quantum Hall insulator physics. The stable superfluidity in the whole ground-state band may lead to other interesting phenomena that have not been explored in regular optical lattices, such as dissipationless Bloch oscillation of BEC.

ACKNOWLEDGMENTS

Y.Z. is supported by ARO (W911NF-09-1-0248) and AFOSR (FA9550-11-1-0313). C.Z. is supported by DARPA-YFA (N66001-10-1-4025), ARO (W911NF-12-1-0334), and NSF-PHY (1104546).

[1] L. D. Landau and E. M. Lifshitz, *Quantum Mechanics: Nonrelativistic Theory* (Pergamon, Oxford, 1977).
[2] A. B. Harris, C. Kallin, and A. J. Berlinsky, Phys. Rev. B **45**, 2899 (1992).
[3] K. Ohgushi, S. Murakami, and N. Nagaosa, Phys. Rev. B **62**, R6065 (2000).
[4] D. Weaire and M. F. Thorpe, Phys. Rev. B **4**, 2508 (1971).
[5] J. P. Straley, Phys. Rev. B **6**, 4086 (1972).
[6] H. Tasaki, Phys. Rev. Lett. **69**, 1608 (1992).
[7] C. Wu, D. Bergman, L. Balents, and S. Das Sarma, Phys. Rev. Lett. **99**, 070401 (2007).
[8] E. Tang, J.-W. Mei, and X.-G. Wen, Phys. Rev. Lett. **106**, 236802 (2011).
[9] K. Sun, Z. Gu, H. Katsura, and S. Das Sarma, Phys. Rev. Lett. **106**, 236803 (2011).
[10] T. Neupert, L. Santos, C. Chamon, and C. Mudry, Phys. Rev. Lett. **106**, 236804 (2011).
[11] D. N. Sheng, Z.-C. Gu, K. Sun, and L. Sheng, Nat. Commun. **2**, 389 (2011).
[12] F. Wang and Y. Ran, Phys. Rev. B **84**, 241103 (2011).
[13] D. Xiao, W. G. Zhu, Y. Ran, N. Nagaosa, and S. Okamoto, Nat. Commun. **2**, 596 (2011).
[14] Y.-F. Wang, Z.-C. Gu, C.-D. Gong, and D. N. Sheng, Phys. Rev. Lett. **107**, 146803 (2011).
[15] Y.-J. Lin, K. Jiménez-García, and I. B. Spielman, Nature (London) **471**, 83 (2011).
[16] J. Dalibard, F. Gerbier, G. Juzeliunas, and P. Öhberg, Rev. Mod. Phys. **83**, 1523 (2011).
[17] C. Wang, C. Gao, C.-M. Jian, and H. Zhai, Phys. Rev. Lett. **105**, 160403 (2010).
[18] T.-L. Ho and S. Zhang, Phys. Rev. Lett. **107**, 150403 (2011).
[19] C. Wu, I. Mondragon-Shem, and X.-F. Zhou, Chin. Phys. Lett. **28**, 097102 (2011).

[20] Y. Zhang, L. Mao, and C. Zhang, Phys. Rev. Lett. **108**, 035302 (2012).
[21] S.-K. Yip, Phys. Rev. A **83**, 043616 (2011).
[22] Z. F. Xu, R. Lü, and L. You, Phys. Rev. A **83**, 053602 (2011).
[23] T. Kawakami, T. Mizushima, and K. Machida, Phys. Rev. A **84**, 011607 (2011).
[24] X.-Q. Xu and J. H. Han, Phys. Rev. Lett. **107**, 200401 (2011).
[25] X.-F. Zhou, J. Zhou, and C. Wu, Phys. Rev. A **84**, 063624 (2011).
[26] J. Radić, T. A. Sedrakyan, I. B. Spielman, and V. Galitski, Phys. Rev. A **84**, 063604 (2011).
[27] S. Sinha, R. Nath, and L. Santos, Phys. Rev. Lett. **107**, 270401 (2011).
[28] H. Hu, B. Ramachandhran, H. Pu, and X.-J. Liu, Phys. Rev. Lett. **108**, 010402 (2012).
[29] Y. Li, L. P. Pitaevskii, and S. Stringari, Phys. Rev. Lett. **108**, 225301 (2012).
[30] T. Ozawa and G. Baym, Phys. Rev. A **85**, 013612 (2012).
[31] B. Ramachandhran, B. Opanchuk, X.-J. Liu, H. Pu, P. D. Drummond, and H. Hu, Phys. Rev. A **85**, 023606 (2012).
[32] Y. Zhang, G. Chen, and C. Zhang, arXiv:1111.4778.
[33] Q. Zhu, C. Zhang, and B. Wu, Europhys. Lett. **100**, 50003 (2012).
[34] E. van der Bijl and R. A. Duine, Phys. Rev. Lett. **107**, 195302 (2011).
[35] J.-Y. Zhang *et al.*, Phys. Rev. Lett. **109**, 115301 (2012).
[36] J. Larson and E. Sjöqvist, Phys. Rev. A **79**, 043627 (2009).
[37] M. Gong, S. Tewari, and C. Zhang, Phys. Rev. Lett. **107**, 195303 (2011).
[38] H. Hu, L. Jiang, X. J. Liu, and H. Pu, Phys. Rev. Lett. **107**, 195304 (2011).
[39] Z.-Q. Yu and H. Zhai, Phys. Rev. Lett. **107**, 195305 (2011).
[40] J. Larson, J. P. Martikainen, A. Collin, and E. Sjöqvist, Phys. Rev. A **82**, 043620 (2010).
[41] R. M. Lutchyn, J. D. Sau, and S. Das Sarma, Phys. Rev. Lett. **105**, 077001 (2010).
[42] Y. Oreg, G. Refael, and F. von Oppen, Phys. Rev. Lett. **105**, 177002 (2010).
[43] N. W. Aschcoft and N. David Mermin, *Solid State Physics* (Saunders College, Philadelphia, 1976).
[44] L. W. Cheuk, A. T. Sommer, Z. Hadzibabic, T. Yefsah, W. S. Bakr, and M. W. Zwierlein, Phys. Rev. Lett. **109**, 095302 (2012).
[45] C. J. Pethick and H. Smith, *Bose-Einstein Condensation in Dilute Gases*, 2nd ed. (Cambridge University Press, Cambridge, UK, 2008).
[46] B. Wu and Q. Niu, Phys. Rev. A **64**, 061603(R) (2001).
[47] B. Wu and Q. Niu, New J. Phys. **5**, 104 (2003).
[48] A. Smerzi, A. Trombettoni, P. G. Kevrekidis, and A. R. Bishop, Phys. Rev. Lett. **89**, 170402 (2002).
[49] M. Machholm, C. J. Pethick, and H. Smith, Phys. Rev. A **67**, 053613 (2003).
[50] S. Burger, F. S. Cataliotti, C. Fort, F. Minardi, M. Inguscio, M. L. Chiofalo, and M. P. Tosi, Phys. Rev. Lett. **86**, 4447 (2001).
[51] L. Fallani, L. De Sarlo, J. E. Lye, M. Modugno, R. Saers, C. Fort, and M. Inguscio, Phys. Rev. Lett. **93**, 140406 (2004).
[52] O. Morsch and M. Oberthaler, Rev. Mod. Phys. **78**, 179 (2006).
[53] S. Hooley and K. A. Benedict, Phys. Rev. A **75**, 033621 (2007).
[54] J. Ruostekoski and Z. Dutton, Phys. Rev. A **76**, 063607 (2007).
[55] A. J. Ferris, M. J. Davis, R. W. Geursen, P. B. Blakie, and A. C. Wilson, Phys. Rev. A **77**, 012712 (2008).
[56] G. Barontini and M. Modugno, Phys. Rev. A **80**, 063613 (2009).
[57] The scattering lengths for different hyperfine spin states are $a_{11} = a_{12} = 100.4a_B$ and $a_{22} = 100.86a_B$ [15] with a_B the Bohr radius. We use typical experimental parameters $\omega_y = \omega_z = 120$ Hz, and the atom number in one unit cell $N = 35$ which corresponds approximately to a 6×10^4 total atom number. The corresponding scale parameters are $c_{11} = c_{12} = 0.0506$, $c_{22} = 0.0508$ and their difference is negligible.